F.E.M. for Prestressed Saint Venant-Kirchhoff Hyperelastic Membranes

Antonio J. Gil

Civil and Computational Engineering Centre, School of Engineering, University of Swansea, Singleton Park, SA2 8PP, United Kingdom a.j.gil@swansea.ac.uk

Summary. *This chapter presents a complete numerical formulation for the nonlinear structural analysis of prestressed membranes with applications in Civil Engineering. These sort of membranes can be considered to undergo large deformations but moderate strains, consequently nonlinear continuum mechanics principles for large deformation of prestressed bodies will be employed in order to proceed with the analysis. The constitutive law adopted for the material will be the one corresponding to a prestressed hyperelastic Saint Venant-Kirchhoff model. To carry out the computational resolution of the structural problem, the Finite Element Method (FEM) will be implemented according to a Total Lagrangian Formulation (TLF), by means of the Direct Core Congruential Formulation (DCCF). Eventually, some numerical examples will be introduced to verify the accuracy and robustness of the aforementioned formulation.*

Key words: Tension membrane structures, Total Lagrangian Formulation, Direct Core Congruential Formulation, Hyperelastic Saint Venant-Kirchhoff material, Newton-Raphson method

1 Introduction

Tension structures constitute a structural form providing remarkable opportunities in the fields of architecture and civil engineering. Nowadays, numerous practical examples can be located throughout the entire world because of the acceptance by designers and their upward trend in popularity -see [1], [2], [3], [4]-. The increasing necessity of creating large enclosed areas, unobstructed by intermediate supports, has allowed the introduction of limitless possibilities for doubly curved surface forms -see [5]-. Although there are several categories that fall into the general term of tension structures, this paper will focus on the well known prestressed membranes, from which prestressed cables can be analyzed by extension. As an instance of these models, Fig. 1 reflects several views of a prestressed cable reinforced membrane.

We will focus on those particular membranes where strains can be assumed moderate, despite having large deformations. Two different and successive loading cases may be distinguished according to their effects on the stabilization of the

E. Oñate and B. Kröplin (eds.), Textile Composites and Inflatable Structures, 123–142.

prestressed membrane. The first one or prestressed loading is developed to provide the necessary in-surface rigidity to the membrane in order to support the second loading step. The latter, also named in service loading step is comprised of a wide group of loads: snow, wind or live loads among others.

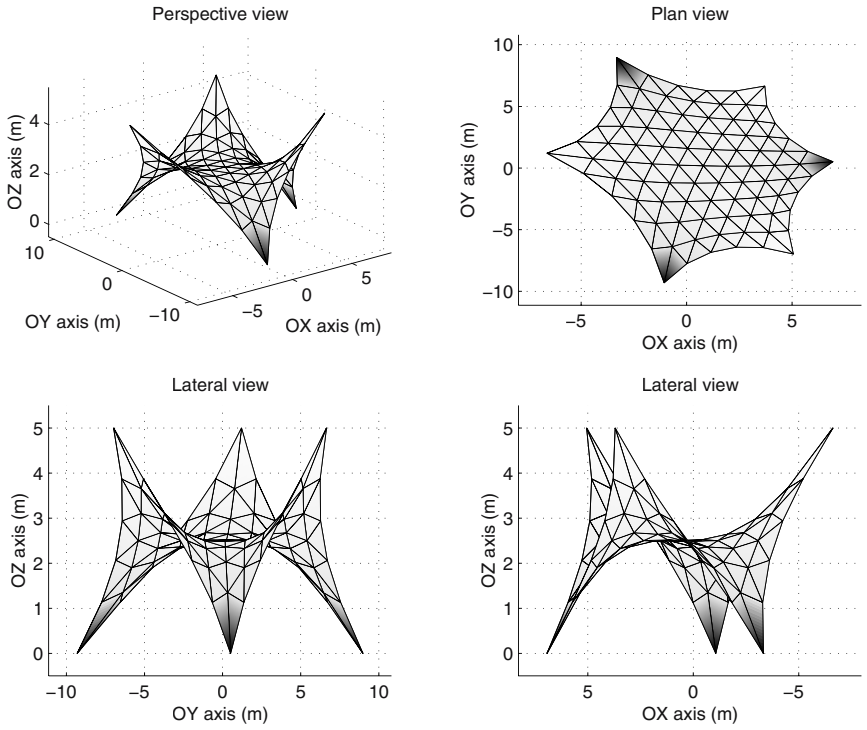

Fig. 1. Prestressed cable reinforced membrane

The theory of hyperelastic membranes, as for instance, propounded by [6], [7] and [8] treats the problem from an analytical point of view. Some simplicity may be accomplished if the Von Karman compatibility equations are used -see [9] and [10]-, whereby rotations are considered to be moderate. Regardless of the important implications of this approach for the theoretical understanding of these structures, a main disadvantage is that it results in a nonlinear partial differential system of equations with impossible analytical resolution.

Because of this lack of numerical results, variational approaches ought to be taken into consideration as the best means to provide feasible solutions. Some authors have treated the problem of finite hyperelasticity set on rubberlike membrane materials by means of the Finite Element Method (FEM). By following this approach, interesting papers are those due to [11], [12], [13], [14], [15] and [16]. For these cases, the Updated Lagrangian Formulation (ULF) is considered to be the most suitable for the derivation of the tangent stiffness matrix. This matrix is re-

quired by the Newton-Raphson iterative scheme for the solution of the nonlinear equilibrium equations.

The discussion to follow is divided into six parts. The second section reviews the classical nonlinear strong form equations. The consideration of the Saint Venant-Kirchhoff material as the adopted model will very conveniently provide a linear constitutive relationship of easy implementation. The third section entails a comprehensive explanation of the Finite Element semidiscretization of the previously obtained strong form. After the weak form is derived in a straightforward manner, the displacement field is interpolated by means of shape functions based on a Lagrangian mesh geometry. The resulting formulation will be the so called Total Lagrangian Formulation (TLF). Afterwards, the exact linearization of the Total Lagrangian weak form of the momentum balance is carried out in detail. For the sake of further computing implementation reasons, the Direct Core Congruential Formulation (DCCF) is reviewed as the most appropriate formulation.

Eventually, based on the aforementioned formulation, two numerical examples for both a cable network and for a prestressed membrane, are presented. These cases will show adequate performance as the required quadratically convergence of the Newton-Raphson method is obtained. Some conclusions are presented at the end.

2 Strong Formulation: General Structural Principles

Before establishing the formulation in terms of particular finite elements, that is, cable or membrane elements, we will develop in this section the general equations that govern the behaviour of prestressed membrane structures. For a complete understanding, it is necessary to consider three successive configurations of the material body: an initial nominally stressed state $\Re_0$, a primary state $\Re_t$ and a secondary state $\Re_{t^*}$, for the time instants t and t^*, respectively. It is important to point out that the term nominally stressed state is employed to describe a self-equilibrated configuration where the internal stresses are as small as required by the designer. Usually, $\Re_0$ represents the nominally stressed state found at a form finding state. $\Re_t$ symbolizes the actual in service prestressed state prior to the live loading, which may be different to $\Re_0$ and due to constructions prestresses. Finally, $\Re_{t^*}$ stands for the live loading in service state.

Between these latter two stages, a displacement field $\mathbf{u} = (u_1, u_2, u_3)$ may be defined in $\mathbf{R}^3$. To differentiate the coordinates of a body particle along the deformation path, the following convention will be employed throughout the remainder of this paper:

- X_A, $(A = 1, 2, 3)$ for the initial nominally stressed configuration $\Re_0$.
- X_j^{pret}, $(j = 1, 2, 3)$ for the initial prestressed configuration $\Re_t$ or primary state.
- x_i, $(i = 1, 2, 3)$ for the current spatial configuration $\Re_{t^*}$ or secondary state.

Henceforth, we will consider as incremental those quantities which proceed from the movement from the primary to the secondary state. The spatial coordinates for the time t^* of a particle can be related to its material coordinates in the initial nominally stressed configuration $\Re_0$ according to the classical mapping equation $x_i = x_i(X_A, t^*)$. By recalling the chain rule, relations among deformation gradient tensors

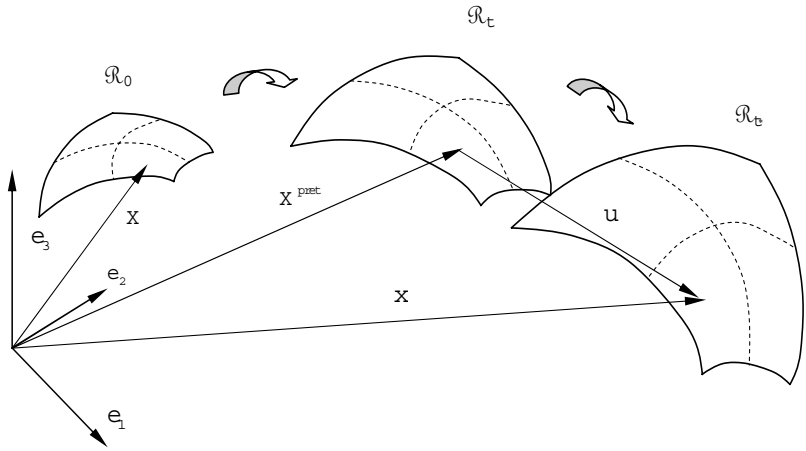

Fig. 2. Deformation path

and their respective jacobians are summarized as:

$$x_{i,A} = x_{i,j} X^{pret}_{j,A} \quad \Rightarrow \quad J^* = J' J \tag{1}$$

where the implied summation convention for repeated indices as well as the comma differentiation symbol $x_{i,j} = \partial x_i / \partial X^{pret}_j$ have been introduced to simplify the algebra. The term J above represents the jacobian at the primary state, J^* stands for the jacobian at the end of the secondary state and $J^{'}$ symbolizes the jacobian as a consequence of the incremental deformation.

The description of the deformation and the measure of strain are essential parts of nonlinear continuum mechanics. From a kinematically point of view, a material particle position in the primary and secondary states may be expressed in terms of the incremental displacement field. Analogously, the deformation gradient tensor may be introduced to characterize adequately the deformation path as:

$$x_i = X^{pret}_i + u_i \quad \Rightarrow \quad x_{i,A} = X^{pret}_{i,A} + u_{i,A} = X^{pret}_{i,A} + u_{i,j} X^{pret}_{j,A} \tag{2}$$

where:

$$u_{i,j} = \frac{\partial u_i}{\partial X^{pret}_j} \tag{3}$$

In contrast to linear elasticity, many different measures of strain may be used in nonlinear continuum mechanics. Nevertheless, the Green-Lagrange strain tensor is considered to be the most appropriate measure specially when dealing with moderate strains. The Green-Lagrange strain tensor for the secondary state with respect to the initial nominally stressed configuration is defined in terms of the deformation gradient tensor and the Delta-Kronecker tensor as:

$$E^*_{AB} = \frac{1}{2}(x_{i,A} x_{i,B} - \delta_{AB}) \tag{4}$$

By substituting equation (2) into equation (4):

$$E^*_{AB} = \frac{1}{2}(X^{pret}_{i,A} X^{pret}_{i,B} - \delta_{AB}) + \frac{1}{2}(2 X^{pret}_{i,A} X^{pret}_{j,B} e_{ij} + u_{i,A} u_{i,B}) \tag{5}$$

with:

$$e_{ij} = \frac{1}{2}(u_{i,j} + u_{j,i}) \tag{6}$$

The difference between the Green-Lagrange strain tensor for the primary and secondary states can be carried out in a straightforward manner as:

$$E^*_{AB} - E_{AB} = X^{pret}_{i,A} X^{pret}_{j,B} e_{ij} + \frac{1}{2} u_{i,A} u_{i,B} \tag{7}$$

By applying the chain rule:

$$E^*_{AB} - E_{AB} = X^{pret}_{i,A} X^{pret}_{j,B} (e_{ij} + \frac{1}{2} u_{s,i} u_{s,j}) = X^{pret}_{i,A} X^{pret}_{j,B} E^{*relat}_{ij} \tag{8}$$

where the tensor E^{*relat}_{ij} has been introduced for the sake of convenience and it represents a relative measure of the strain at the secondary state by taking the primary one as an adequate reference.

In nonlinear problems, various stress measures can be defined. In this paper, in addition to the Cauchy or real stress tensor, two tensorial entities referred to as the second Piola-Kirchhoff and the nominal stress tensors are to be used. The latter is known as well as the transpose of the first Piola-Kirchhoff stress tensor. By considering as initial configuration the initial nominally stressed one, the Cauchy stress tensor σ^*_{ij} may be related to the nominal stress tensor P^*_{Aj} and the second Piola-Kirchhoff stress tensor S^*_{AB} as:

$$J^* \sigma^*_{ij} = x_{i,A} P^*_{Aj} = x_{i,A} x_{j,B} S^*_{AB} \qquad x_{i,A} = \frac{\partial x_i}{\partial X_A} \tag{9}$$

The same relationship may be developed when the initial prestressed configuration is adopted to be the reference state. The super index *relat* is added to distinguish the new nonlinear stress tensors with respect to those shown in the above formula:

$$J' \sigma^*_{ij} = x_{i,s} P^{*relat}_{sj} = x_{i,s} x_{j,t} S^{*relat}_{st} \qquad x_{i,s} = \frac{\partial x_i}{\partial X^{pret}_s} \tag{10}$$

Formulae (9) and (10) can be modified to set up expressions (11) which summarize the relationship among the nominal and second Piola-Kirchhoff stress tensors obtained in both the initial undeformed configuration $\Re_0$ and the primary state $\Re_t$.

$$\begin{aligned} P^{*relat}_{sj} &= J^{-1} X^{pret}_{s,A} X^{pret}_{t,B} x_{j,t} S^*_{AB} \\ S^{*relat}_{st} &= J^{-1} X^{pret}_{s,A} X^{pret}_{t,B} S^*_{AB} \end{aligned} \tag{11}$$

The local equilibrium equations in the secondary state may be expressed with respect to three possible descriptions: $\Re_0$, $\Re_t$ and $\Re_{t^*}$, these being a Lagrangian formulation for the first two configurations and an Eulerian formulation for the final configuration. These expressions may be gathered as follows:

$$\sigma^*_{ji,j} + \rho^* b_i = 0 \ \text{ in } \ \Re_{t^*}, \ \text{ with } f^*_i = \sigma^*_{ji} n^*_j d\Gamma^* \tag{12}$$

$$P^*_{Ai,A} + \rho_0 b_i = 0 \ \text{ in } \ \Re_0, \ \text{ with } f^*_i = P^*_{Ai} n_A d\Gamma_0 \tag{13}$$

$$P^{*relat}_{ji,j} + \rho b_i = 0 \ \text{ in } \ \Re_t, \ \text{ with } \ f^*_i = P^{*relat}_{ji} n_j d\Gamma \tag{14}$$

The formula (14) along with the boundary conditions and continuity conditions -see [17]-, represents the strong formulation of the structural problem according to a Lagrangian description with respect to a reference stressed configuration. This is the equation that will be used from now on.

Many engineering applications, particularly the one which concerns us, involve moderate strains and large rotations. Therefore, in these kind of problems the effects of large deformation are primarily due to rotations. The response of the material may then be modeled as an extension of the well known linear elastic law by replacing the Cauchy stress tensor by the second Piola-Kirchhoff stress one and the small strain tensor by the Green-Lagrange strain one.

This material behaviour is named Saint Venant-Kirchhoff hyperelastic or simply Kirchhoff material. By accounting for the hyperelastic pattern of this constitutive model, the second Piola-Kirchhof stress tensor may be formulated in an elegant way by means of the Helmholtz free energy -also known as internal strain energy-. Thus, the second Piola-Kirchhoff stress tensor in the current configuration may be formulated by means of a Taylor series expansion truncated after the first order as follows:

$$S^*_{AB} = \frac{\partial w_{int}}{\partial E^*_{AB}} = \frac{\partial w_{int}}{\partial E_{AB}} + \frac{\partial^2 w_{int}}{\partial E_{AB} \partial E_{CD}} (E^*_{CD} - E_{CD}) \tag{15}$$

The accuracy of this Taylor series depends directly on the smallness of the step $E^*_{CD} - E_{CD}$. For tension membrane structures, as it was previously mentioned, this is a valid assumption. Thus:

$$S^*_{AB} = S_{AB} + C_{ABCD} X^{pret}_{i,C} X^{pret}_{j,D} E^{*relat}_{ij} \tag{16}$$

By recalling (11) and (16):

$$S^{*relat}_{st} = J^{-1} X^{pret}_{s,A} X^{pret}_{t,B} S_{AB} + J^{-1} X^{pret}_{s,A} X^{pret}_{t,B} C_{ABCD} X^{pret}_{i,C} X^{pret}_{j,D} E^{*relat}_{ij} \tag{17}$$

The fourth order tensor of elastic moduli can be referred to the prestressed configuration as follows:

$$C_{ijkl} = J^{-1} X^{pret}_{i,A} X^{pret}_{j,B} C_{ABCD} X^{pret}_{k,C} X^{pret}_{l,D} \tag{18}$$

Eventually, equation (17) may be reformulated to give the final expression:

$$S^{*relat}_{ij} = \sigma_{ij} + C_{ijkl} E^{*relat}_{kl} \tag{19}$$

This final formula is set up to show the constitutive law for a prestressed Saint Venant-Kirchhoff hyperelastic material. The second Piola-Kirchhoff stress tensor is expressed in terms of an easy linear relationship which depends on three tensorial entities: Cauchy stress tensor in the primary state, fourth order tensor of elastic moduli and the Green-Lagrange strain tensor of the secondary state referred to the primary state.

Recall -see [18]- that in a Saint Venant-Kirchhoff hyperelastic material, the constitutive tensor can be formulated as follows:

$$C_{ijkl} = \lambda \delta_{ij} \delta_{kl} + 2\mu \delta_{ik} \delta_{jl} \tag{20}$$

where λ and μ are known as the Lamé constants. These two constants can be related to the classical Young modulus E and Poisson's ratio ν as follows:

$$\lambda = \frac{\nu E}{(1+\nu)(1-2\nu)} \qquad \mu = \frac{E}{2(1+\nu)} \tag{21}$$

Another important feature which needs to be obtained is the incremental strain energy accumulated into the structure along the deformation path from the primary to the secondary states. By performing again a Taylor series expansion truncated after the second order, the internal strain energy functional per unit of nominally stressed volume may be developed as:

$$w^*_{int} = w_{int} + \frac{\partial w_{int}}{\partial E_{AB}}(E^*_{AB} - E_{AB}) + \frac{1}{2}\frac{\partial^2 w_{int}}{\partial E_{AB}\partial E_{CD}}(E^*_{AB} - E_{AB})(E^*_{CD} - E_{CD}) \tag{22}$$

This above formula can be rewritten as:

$$w^*_{int} = w_{int} + \Omega + \Upsilon \tag{23}$$

where the terms Ω and Υ can be depicted as:

$$\Omega = S_{AB} X^{pret}_{i,A} X^{pret}_{j,B} E^{*relat}_{ij} = J\sigma_{ij} E^{*relat}_{ij} \tag{24}$$

$$\Upsilon = \frac{1}{2} C_{ABCD} X^{pret}_{i,A} X^{pret}_{j,B} E^{*relat}_{ij} X^{pret}_{k,C} X^{pret}_{l,D} E^{*relat}_{kl} = \frac{1}{2} J C_{ijkl} E^{*relat}_{ij} E^{*relat}_{kl} \tag{25}$$

By substituting (24) and (25) back into (22):

$$w^*_{int} - w_{int} = J[\sigma_{ij} E^{*relat}_{ij} + \frac{1}{2} C_{ijkl} E^{*relat}_{ij} E^{*relat}_{kl}] = J\Psi \tag{26}$$

By integrating over the initial undeformed volume V^0 corresponding to the configuration $\Re_0$, and by applying the mass conservation principle from this volume V^0 to the prestressed volume V^{pret} corresponding to the configuration $\Re_t$, we obtain the incremental Helmholtz's free energy functional, which is given as:

$$\Delta W_{int} = \int_{V^0} (w^*_{int} - w_{int}) dV = \int_{V^0} J\Psi dV = \int_{V^{pret}} \Psi dV = \int_{V^{pret}} w^{*relat}_{int} dV \tag{27}$$

Therefore, the internal strain energy functional per unit of volume of the primary state takes the final form:

$$w^{*relat}_{int} = \sigma_{ij} E^{*relat}_{ij} + \frac{1}{2} C_{ijkl} E^{*relat}_{ij} E^{*relat}_{kl} \tag{28}$$

3 Finite Element Discretization

3.1 From the Strong to the Weak Formulation

The above mentioned primary and secondary states can be understood as an initial prestressed state $\Re^{pret}$ and a final in service loading state $\Re$ due to the consideration of live and dead load. Henceforth, the coordinates of any body's particle, in

both prestressed and final loaded states, are related by means of the incremental displacement field $\mathbf{u}$ as follows:

$$\mathbf{x} = \mathbf{X}^{pret} + \mathbf{u}, \quad x_i = X_i^{pret} + u_i \tag{29}$$

According to this nomenclature, the strong formulation of the problem in a Lagrangian description with respect to the prestressed configuration is summarized in Fig. 3. The configurations $\Re^{pret}$ represents a material body of domain V^{pret} with frontier Γ^{pret}. As can be observed, the super index $*^{relat}$ has been suppressed for the sake of simplicity.

1. Balance of linear momentum.

$$\frac{\partial P_{ji}}{\partial X_j^{pret}} + \rho^{pret} b_i = 0 \;\; in \;\; V^{pret} \tag{30}$$

2. Transformation of stress tensors.

$$J\sigma_{ij} = \frac{\partial x_i}{\partial X_s^{pret}} P_{sj} = \frac{\partial x_i}{\partial X_s^{pret}} \frac{\partial x_j}{\partial X_t^{pret}} S_{st} \;\; \text{with} \;\; J = det(\frac{\partial x_i}{\partial X_j^{pret}}) \tag{31}$$

3. Green-Lagrange strain tensor.

$$E_{ij} = \frac{1}{2}(\frac{\partial x_k}{\partial X_i^{pret}} \frac{\partial x_k}{\partial X_j^{pret}} - \delta_{ij}) \tag{32}$$

4. Constitutive law.

$$S_{ij} = \sigma_{ij}^{pret} + C_{ijkl} E_{kl} \tag{33}$$

5. Internal strain energy functional per unit volume of prestressed configuration.

$$w_{int} = \sigma_{ij}^{pret} E_{ij} + \frac{1}{2} C_{ijkl} E_{ij} E_{kl} \tag{34}$$

6. Boundary conditions.

$$t_i = P_{ji} n_j^{pret} = \bar{t}_i \;\; on \;\; \Gamma_{t_i}^{pret} \qquad u_i = \bar{u}_i \;\; on \;\; \Gamma_{u_i}^{pret} \tag{35}$$

Fig. 3. Strong formulation for a Lagrangian description.

Thus, the weak form may be developed in a Total Lagrangian Format (TLF) by means of the so called Principle of Virtual Work. By neglecting inertia forces:

$$\delta W_{int}(\delta u_i, u_i) = \delta W_{ext}(\delta u_i, u_i) \tag{36}$$

$$\delta W_{int} = \int_{V^{pret}} \delta F_{ij} P_{ji} dV = \int_{V^{pret}} \delta \mathbf{F}^T : \mathbf{P} dV = \int_{V^{pret}} \delta E_{ij} S_{ij} dV = \int_{V^{pret}} \delta \mathbf{E} : \mathbf{S} dV \tag{37}$$

$$\delta W_{ext} = \int_{V^{pret}} \delta u_i b_i dV + \int_{\Gamma^{pret}} \delta u_i \bar{t}_i d\Gamma = \int_{V^{pret}} \delta \mathbf{u}^T \cdot \mathbf{b} dV + \int_{\Gamma^{pret}} \delta \mathbf{u}^T \cdot \bar{\mathbf{t}} d\Gamma \tag{38}$$

where the work conjugacy property of the tensors $\mathbf{S}$ and $\mathbf{P}$ with $\mathbf{E}$ and $\mathbf{F}^T$ respectively, has been employed for the equalities in (37); $\mathbf{b}$ is the body force vector and $\overline{\mathbf{t}}$ are the surface tractions.

3.2 Semidiscretization of the Weak Form

The weak form equations obtained formerly may be combined with a finite element discretization of the displacement field in terms of the nodal values $\mathbf{u}^I$ and shape functions N^I as:

$$u_i = {u_i}^I N^I \quad i = 1, 2, 3; \quad I = 1 \dots N \tag{39}$$

enables the nodal equivalent internal and external vector forces, $\mathbf{f}_{int}$ and $\mathbf{f}_{ext}$, respectively, to be obtained in a straightforward manner for a given node I as:

$$f^I_{int,i} = \int\limits_{V^{pret}} P_{ji} \frac{\partial N^I}{\partial X^{pret}_j} dV = \int\limits_{V^{pret}} F_{ik} S_{kj} \frac{\partial N^I}{\partial X^{pret}_j} dV \tag{40}$$

$$f^I_{ext,i} = \int\limits_{V^{pret}} b_i N^I dV + \int\limits_{\Gamma^{pret}} \bar{t}_i N^I d\Gamma \tag{41}$$

Assembling these forces for all the nodes of the Lagrangian mesh gives the global equilibrium equations:

$$\mathbf{f}_{int} = \mathbf{f}_{ext} \implies \mathbf{f}_{res} = \mathbf{f}_{int} - \mathbf{f}_{ext} = \mathbf{0} \tag{42}$$

where $\mathbf{f}_{int}$ is the global vector of internal forces, $\mathbf{f}_{ext}$ is the global vector of external forces and $\mathbf{f}_{res}$ is the global vector of residual forces. This last vector represents clearly the out of balance forces as a result of the strong nonlinearity contained into the structural problem.

3.3 Linearization of the Global Equilibrium Equations

The set of equations depicted by (42) presents a geometrically nonlinear feature, so an iterative solution scheme will be required. Among all the available methods, the second-order Newton-Raphson one accomplishes the best convergence properties. The total tangent stiffness matrix required by the later one is formed by linearizing the global equilibrium equations (42) in the direction of the incremental displacement $\mathbf{u}$.

By carrying out the linearization of the global vector of internal forces, it turns out to be:

$$d\mathbf{f}^I_{int} = d\mathbf{f}^{mat^I}_{int} + d\mathbf{f}^{geo^I}_{int} = (\mathbf{K}^{mat^{IJ}} + \mathbf{K}^{geo^{IJ}}) d\mathbf{u}^J \tag{43}$$

$$K^{mat^{IJ}}_{ij} = \int\limits_{V^{pret}} F_{ik} \frac{\partial N^I}{\partial X_p} C_{pklm} F_{jl} \frac{\partial N^J}{\partial X_m} dV \tag{44}$$

$$K^{geo^{IJ}}_{ij} = \delta_{ij} \int\limits_{V^{pret}} \frac{\partial N^I}{\partial X_l} S_{lk} \frac{\partial N^J}{\partial X_k} dV \tag{45}$$

where $\mathbf{K}^{mat^{IJ}}$ and $\mathbf{K}^{geo^{IJ}}$ stand for the elemental material or constitutive stiffness matrix and the elemental geometrical or initial stress stiffness matrix, respectively.

By assuming that the body forces $\mathbf{b}$ and external surface tractions $\bar{\mathbf{t}}$ not associated to pressure forces remain constant and by taking into account that the pressure component is dependent upon the geometry due to changing orientation and surface area of the structure, the linearization of the global vector of external forces is given through the following derivation:

$$\mathbf{f}^I_{ext} = \int_\Gamma \mathbf{t} N^I d\Gamma = -p \int_\Gamma \mathbf{n} N^I d\Gamma \tag{46}$$

By applying the Nanson rule for the unit normal $\mathbf{n}$ -see for instance [17] or [19] for details- and particularizing for an isoparametric three-node linear finite element:

$$\mathbf{f}^I_{ext} = -p \int_{\Gamma^{pret}} J\mathbf{F}^{-T}\mathbf{n}^{pret} N^I d\Gamma = \frac{-p\Gamma^{pret}}{3}\left(\frac{\partial \mathbf{x}}{\partial \xi_1^{pret}} \times \frac{\partial \mathbf{x}}{\partial \xi_2^{pret}}\right) \tag{47}$$

$$K^{p^{IJ}}_{ij} = \frac{-p\Gamma^{pret}\epsilon_{ilm}}{3}\left(\delta_{lj}\frac{\partial N^J}{\partial \xi_1^{pret}} F_{m2} + F_{l1}\delta_{mj}\frac{\partial N^J}{\partial \xi_2^{pret}}\right) \tag{48}$$

where p is the pressure scalar acting on the considered finite element, ξ_1^{pret} and ξ_2^{pret} are the local plane coordinates and $\boldsymbol{\epsilon}$ is the so called alternating third order tensor.

3.4 Direct Core Congruential Formulation (DCCF)

From the computational viewpoint, a very elegant procedure termed the Direct Core Congruential Formulation (DCCF) may be applied to perform the implementation stage of the formulation developed above. This methodology, which is hardly used in the existing literature is due to pioneer studies in [20] and [21]. The main ideas behind this formulation can be discovered in the notable paper due to [22].

The scope of the DCCF is establishing the set of global equilibrium equations whose unknowns are the components of the displacement gradient tensor $\mathbf{G}$ which is given as:

$$G_{ij} = \frac{\partial u_i}{\partial X_j^{pret}} \tag{49}$$

Therefore, this new set of equations is completely independent on the geometry of the structure and on the adopted discretization properties. Afterwards, every single component of the displacement gradient tensor may be easily expressed in terms of the nodal displacements of the Lagrangian mesh. Naturally, it is right then when properties concerning geometry and discretization are brought to light. The consideration of only traslational degrees of freedom for the nodes of the Lagrangian mesh makes the DCCF specially simple and easy of being implemented. The Fig. 4 shows a summary of this formulation:

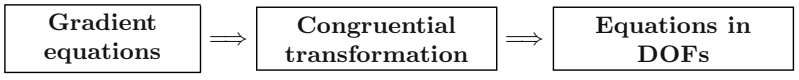

Fig. 4. DCCF scheme.

By employing a classical vectorization of the displacement gradient tensor -see for instance [17] and [19]- into a column vector $\mathbf{g}$ and by expressing this in terms of the nodal displacements, it turns:

$$\mathbf{g} = \mathbf{B}\mathbf{u} \tag{50}$$

where $\mathbf{B}$ is the matrix of the gradients of the shape functions for the chosen finite element and $\mathbf{u}$ is the column vector that gathers the nodal displacements for the N nodes of a single finite element:

$$\mathbf{u}^T = \begin{pmatrix} u_1^1 & u_2^1 & u_3^1 & \dots & u_1^N & u_2^N & u_3^N \end{pmatrix} \tag{51}$$

Analogously, the 2x2 submatrix of in-plane components of the Green-Lagrange strain tensor $\mathbf{E}$ may be vectorized into a column vector $\mathbf{e}$ by following the kinematic Voigt rule as:

$$\mathbf{e}^T = \begin{pmatrix} E_{11} & E_{22} & 2E_{12} \end{pmatrix} \tag{52}$$

Every component of the new vector $\mathbf{e}$ may be expressed in terms of the vector $\mathbf{g}$ as:

$$e_i = \mathbf{h}_i^T \mathbf{g} + \frac{1}{2}\mathbf{g}^T \mathbf{H}_i \mathbf{g} \tag{53}$$

where $\mathbf{h}_i$ and $\mathbf{H}_i$ are a vector and a symmetric matrix of numerical values comprising $(1, 0)$. Eventually, the in-plane components of the second Piola-Kirchhoff stress tensor may be transformed into a vector by means of the kinetic Voigt rule as:

$$\mathbf{s}^T = \begin{pmatrix} S_{11} & S_{22} & S_{12} \end{pmatrix} \tag{54}$$

By substituting equations (53) and (54) back into (37) the vector of global internal forces may be rewritten in an easier way as:

$$\mathbf{f}_{int} = \int\limits_{V^{pret}} \mathbf{B}^T \boldsymbol{\phi}_{int} dV \qquad \boldsymbol{\phi}_{int} = s_i \mathbf{h}_i + s_i \mathbf{H}_i \mathbf{g} \tag{55}$$

where summation is implied for repeated indices according to Einstein's notation. By proceeding in the same manner, the contributions to the generic total tangent stiffness matrix $\mathbf{K}^{mat}$ and $\mathbf{K}^{geo}$ may be obtained as:

$$\mathbf{K}^{mat} = \int\limits_{V^{pret}} \mathbf{B}^T \mathbf{S}^{mat} \mathbf{B} dV \qquad \mathbf{K}^{geo} = \int\limits_{V^{pret}} \mathbf{B}^T \mathbf{S}^{geo} \mathbf{B} dV \tag{56}$$

$$\mathbf{S}^{mat} = (\mathbf{h}_i + \mathbf{H}_i \mathbf{g}) C_{ij} (\mathbf{h}_j^T + \mathbf{g}^T \mathbf{H}_j) \qquad \mathbf{S}^{geo} = s_i \mathbf{H}_i \tag{57}$$

where the fourth order tensor of elastic moduli, C_{ij}, has been transformed into a 3x3 matrix by applying the Voigt rule vectorization procedure to equation (33) to come out with:

$$\mathbf{s} = \boldsymbol{\sigma}^{\boldsymbol{pret}} + \mathbf{C}\mathbf{e} \tag{58}$$

In the next sections, two numerical examples will be presented with the purpose of demonstrating the capabilities of the described technique. The Finite Element Method was applied to study both a prestressed cable network and a prestressed membrane. As a consequence, the DCCF was particularized on two different finite elements: a two-noded and a three-noded linear isoparametric finite elements. The latter is described in some detail in the appendix located at the end of the chapter.

4 Numerical Example: Cable Network

This example, extracted from [23], represents a squared hyperbolic paraboloid with a 12 foot horizontal side. The difference between the highest and lowest points is measured as 1.5 feet. The sides of the structural model are composed of rigid beams which prevent any displacement.

The structure is modelled by means of a cable network depicted at Fig. 5, where a representation of nodes and elements can be observed. The external nodes are adopted to be fixed and the only allowed displacement is for the inner nodes.

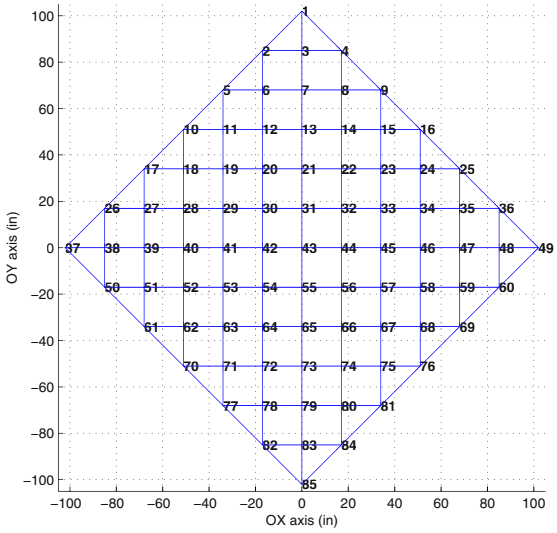

Fig. 5. Broughton: cable discretization.

All the cables are subjected to a previous prestressed state of 1.2 Kip. In addition to that, the cables will be represented by a unique material of $0.618e3$ Kip for the mechanical factor EA.

The structural model undergoes under service conditions a downward point load of value 0.22 Kip applied at node 79 -see figure (5)-. The analysis has been solved by using a Newton-Raphson numerical scheme in one incremental step.

Figs. 6 and 7 represent both original and displaced shapes. Analogously, Table 1 reflects a survey of displacements according to the different spatial directions for some remarkable internal nodes. Results according to reference [23] and present work are displayed.

Fig. 8 gathers the convergence curves for the numerical method which has been employed. Eventually, a representation of the Cauchy axial forces is shown in Fig. 9.

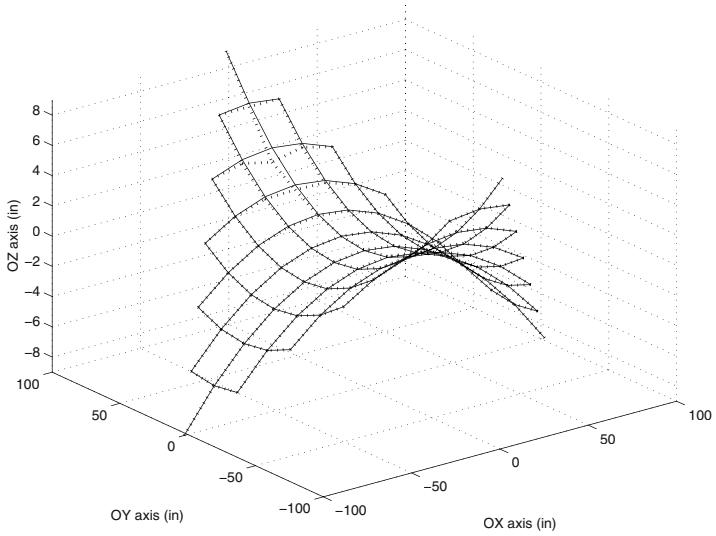

Fig. 6. Structural model: cable isometric view.

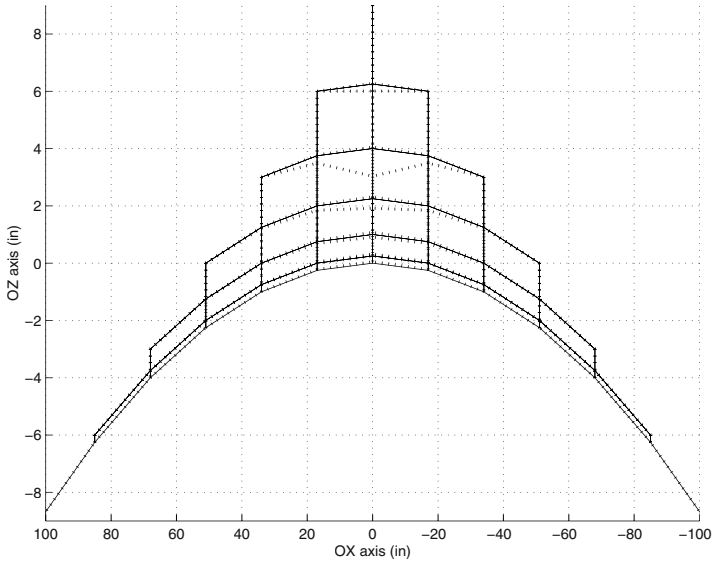

Fig. 7. Structural model: cable lateral view.

5 Numerical Example: Membrane

This example is considered in [24]. It is a square plane membrane initially prestressed. The edges of the membrane are completely fixed. The side length is 240 in and the thickness is measured as 0.004167 in. Mechanical properties for the ma-

	Broughton			Present work		
Node	u	v	w	u	v	w
83	0.0000	-0.0334	-0.2410	0.0000	-0.0340	-0.2415
79	0.0000	-0.1390	-0.9650	0.0000	-0.1388	-0.9667
43	0.0000	-0.0410	0.0510	0.0000	-0.0414	0.0516
23	0.0000	-0.0020	0.0160	-0.0002	-0.0016	0.0155

Table 1. Displacements (in).

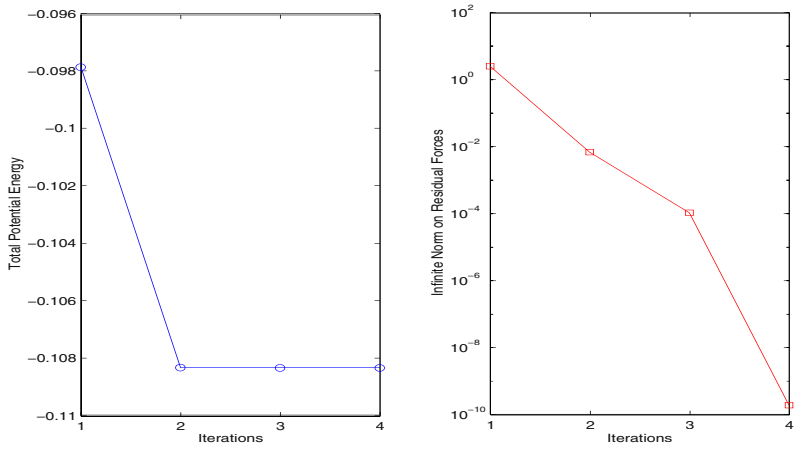

Fig. 8. Convergence curves.

terial are adopted to have the following values: 30,000 Ksi for the Young modulus and 0.3 for the Poisson ratio. The prestressing effect is considered to be 80,000 psi isotropically distributed. The mesh adopted is the same as the one employed in the original reference for the sake of comparison purposes. More accurate results would have been achieved with a finer mesh.

In service loading conditions are taken to be a point transverse load applied in middle. The load which takes a value of 10 Kip is taken downwards. According to the Fig. 10, the Lagrangian mesh is comprised of 32 isoparametric three-node linear elements and 25 nodes.

To accomplish the final solution, the employed method was the Newton-Raphson method for a single load increment. Two convergence curves are gathered in Fig. 11. The first shows the evolution of the total potential energy along the iterations path, whilst the second represents the infinite norm on residual forces vector with respect to the number of iterations as well. The second curve shows perfectly the required quadratic convergence of the Newton-Raphson algorithm.

Fig. 12 shows the displacement field along the cartesian axis OX and OZ, respectively. Both representations reveal in a clear manner the axisymmetry of the membrane. Table 2 details the displacement values for three different nodes of the mesh. The accuracy of the numerical example can be observed by checking the results with those obtained in [24].

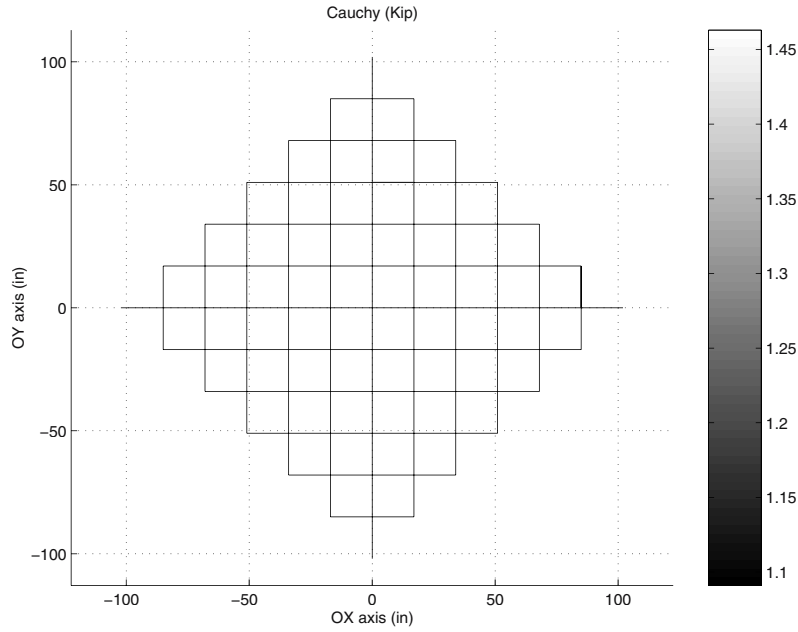

Fig. 9. Axial forces(Kip).

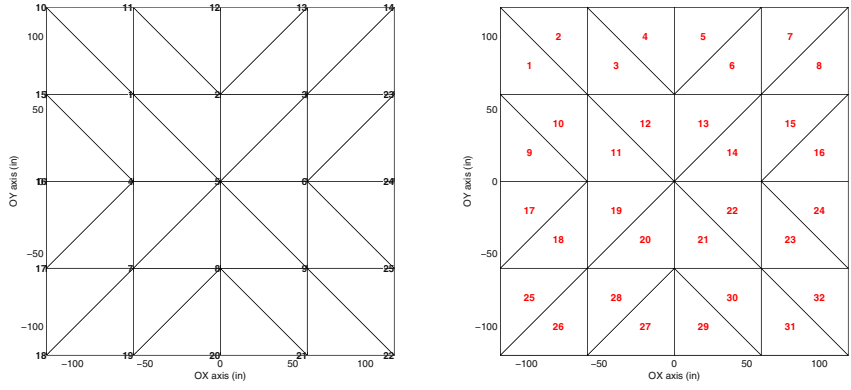

Fig. 10. Numerical example: Discretization.

Analogously, principal Cauchy stresses σ_I and σ_{II} can be viewed in Fig. 13. Table 3 presents the numerical values for three different elements of the membrane as well as its comparison with those of [24]. Perfect agreement can be deduced.

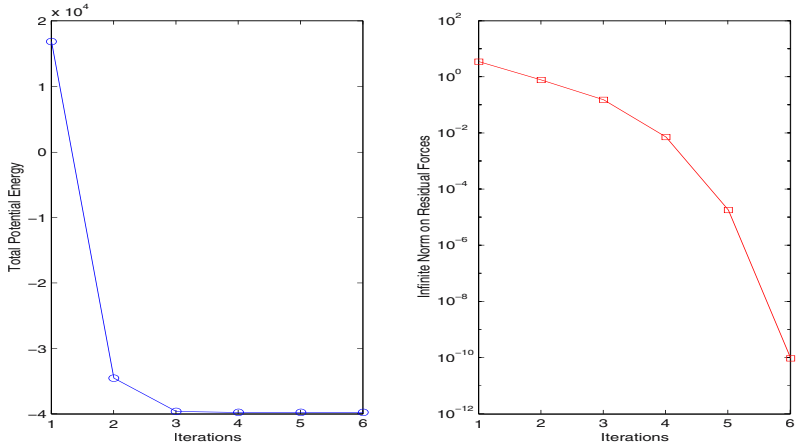

Fig. 11. Numerical example: Convergence curves.

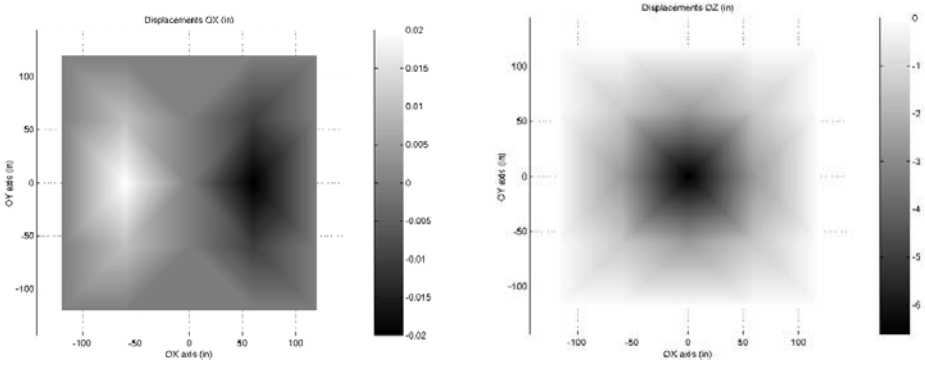

Fig. 12. Numerical example: Displacements OX & OZ.

	Levy & Spillers			Present work		
Node	u	v	w	u	v	w
1	0.015	-0.015	-1.431	0.014	-0.014	-1.423
2	0.000	-0.017	-2.605	0.000	-0.017	-2.600
5	0.000	0.000	-6.642	0.000	0.000	-6.626

Table 2. Numerical example: Displacements (in).

6 Concluding Remarks

This chapter has offered a complete consistent numerical formulation for the structural analysis of prestressed hyperelastic Saint Venant-Kirchoff membranes. Two structural loading steps can be considered successively: in the first, the prestressing loads are transferred to the structure whereas in the second, in service loads such as live loads or wind load arise. By taking into account this approach, an initial

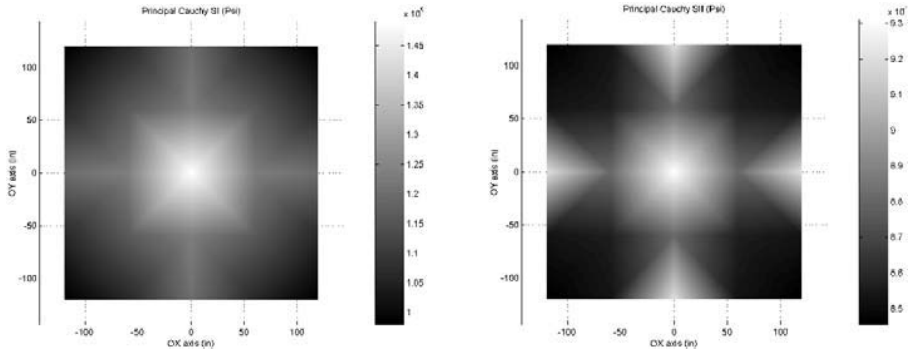

Fig. 13. Numerical example: Cauchy stresses σ_I & σ_{II}.

	Levy & Spillers			Present work		
Element	σ_{xx}	σ_{yy}	σ_{xy}	σ_{xx}	σ_{yy}	σ_{xy}
1	97377.6	85212.4	-2801.5	97300.1	85163.9	-2796.7
3	83510.2	96859.1	-8657.1	83501.5	96830.3	-8630.7
11	144691.0	97830.7	-15615.6	144470.8	97849.2	-15582.4

Table 3. Numerical example 1: Cauchy stresses (Psi).

prestressed configuration can be used to refer all the in service conditions back to it. A Total lagrangian Formulation was developed because of its implicit features. Afterwards, a finite element spatial discretization scheme along with a linearization or perturbation technique were employed over the equivalent internal nodal forces to derive the total tangent stiffness matrix. A straightforward computational implementation is allowed by means of the Direct Core Congruential Formulation. Eventually, the robustness of the whole formulation has been demonstrated by the convergence achievement of some examples.

7 Acknowledgments

I would like to emphasize my gratitude to Professor J. Bonet and Dr. Richard D. Wood, at the Civil and Computational Engineering Centre, University of Swansea, for many helpful comments and discussions.

A.1 Appendix: Three-Node Isoparametric Linear Finite Element

To reduce the continuously distributed structural system to a discrete one, the membrane is approximated by a discrete model consisting of a finite number *elem* of flat three-node isoparametric elements with linear shape functions. The geometry of each

element in the initial prestressed state is thus defined by a plane of uniform thickness t bounded by straight lines which intersects at three points called nodes.

A fixed local coordinate system $O\xi_1^{pret}\xi_2^{pret}\xi_3^{pret}$, in addition to the global reference frame, is established for each element. The behaviour of each element is to be first described independently in terms of its local coordinates and is then to be transformed into global coordinates. For the sake of simplicity, it is assumed that each element lies in the $O\xi_1^{pret}\xi_2^{pret}$ plane of its local coordinate system. The shape functions are evaluated to obtain:

$$N^I(\xi_1^{pret},\xi_2^{pret}) = \tfrac{1}{2\Gamma^{pret}}(a^I + b^I\xi_1^{pret} + c^I\xi_2^{pret})$$

$$a^I = \xi_1^{pret^J}\xi_2^{pret^K} - \xi_1^{pret^K}\xi_2^{pret^J} \quad b^I = \xi_2^{pret^J} - \xi_2^{pret^K} \quad c^I = \xi_1^{pret^K} - \xi_1^{pret^J}$$

$$\Gamma^{pret} = \tfrac{1}{2}(c^K b^J - c^J b^K) \qquad I,J,K = 1,2,3 \tag{A.1}$$

where Γ^{pret} is the area of the initial prestressed triangle. Note that the quantities a^I, b^I and c^I -named Zienkiewicz's coefficients, see for instance [24]- are independent of the deformation of the membrane and are computed directly from the geometry of the initially prestressed shape. According to the Direct Core Congruential Formulation, the vectorized displacement gradient tensor is given in its transpose form as:

$$\mathbf{g}^T = \begin{pmatrix} g_1 & g_2 & g_3 & g_4 & g_5 & g_6 & g_7 & g_8 & g_9 \end{pmatrix}$$

$$\mathbf{g}^T = \begin{pmatrix} \frac{b^I u_1^I}{2\Gamma^{pret}} & \frac{b^I u_2^I}{2\Gamma^{pret}} & \frac{b^I u_3^I}{2\Gamma^{pret}} & \frac{c^I u_1^I}{2\Gamma^{pret}} & \frac{c^I u_2^I}{2\Gamma^{pret}} & \frac{c^I u_3^I}{2\Gamma^{pret}} & 0 & 0 & 0 \end{pmatrix} \tag{A.2}$$

The vector of global internal forces is particularized for the triangular flat element by using the DCCF as:

$$\mathbf{f}_{int} = t\Gamma^{pret}\mathbf{B}^T\boldsymbol{\phi}_{int} = \frac{t}{2}\begin{pmatrix} b^1\mathbf{I}_3 & c^1\mathbf{I}_3 \\ b^2\mathbf{I}_3 & c^2\mathbf{I}_3 \\ b^3\mathbf{I}_3 & c^3\mathbf{I}_3 \end{pmatrix}\boldsymbol{\phi}_{int} \tag{A.3}$$

where:

$$\boldsymbol{\phi}_{int} = s_i\mathbf{h}_i + s_i\mathbf{H}_i\mathbf{g} = \begin{pmatrix} s_1(1+g_1) + s_3 g_4 \\ s_1 g_2 + s_3(1+g_5) \\ s_1 g_3 + s_3 g_6 \\ s_2 g_4 + s_3(1+g_1) \\ s_2(1+g_5) + s_3 g_2 \\ s_2 g_6 + s_3 g_3 \end{pmatrix} \tag{A.4}$$

The total tangent stiffness matrix may be computed by means of the congruential transformation and thus the submatrix due to the contribution of the nodes I and J is depicted as:

$$\mathbf{K}^{IJ} = \frac{t}{4\Gamma^{pret}}(b^I b^J\mathbf{S}_{11} + c^I c^J\mathbf{S}_{22} + b^I c^J\mathbf{S}_{12} + c^I b^J\mathbf{S}_{21} \tag{A.5}$$

where:

$$\mathbf{S}_{ij} = \mathbf{S}_{ij}^{geo} + \mathbf{S}_{ij}^{mat} \qquad i,j = 1,2 \tag{A.6}$$

The geometrical and material components of the stiffness matrix $\mathbf{S}$ can be developed as follows:

$$\mathbf{S}^{geo} = \begin{pmatrix} \mathbf{S}_{11}^{geo} & \mathbf{S}_{12}^{geo} \\ \mathbf{S}_{21}^{geo} & \mathbf{S}_{22}^{geo} \end{pmatrix} \qquad \mathbf{S}^{mat} = \begin{pmatrix} \mathbf{S}_{11}^{mat} & \mathbf{S}_{12}^{mat} \\ \mathbf{S}_{21}^{mat} & \mathbf{S}_{22}^{mat} \end{pmatrix} \tag{A.7}$$

$$\mathbf{S}_{11}^{geo} = s_1\mathbf{I}_3 \qquad \mathbf{S}_{11}^{mat} = C_{11}\mathbf{f}_1\mathbf{f}_1^T + C_{33}\mathbf{f}_2\mathbf{f}_2^T + C_{13}\mathbf{f}_1\mathbf{f}_2^T + C_{31}\mathbf{f}_2\mathbf{f}_1^T \tag{A.8}$$

$$\mathbf{S}_{12}^{geo} = s_3\mathbf{I}_3 \qquad \mathbf{S}_{12}^{mat} = C_{13}\mathbf{f}_1\mathbf{f}_1^T + C_{32}\mathbf{f}_2\mathbf{f}_2^T + C_{12}\mathbf{f}_1\mathbf{f}_2^T + C_{33}\mathbf{f}_2\mathbf{f}_1^T \tag{A.9}$$

$$\mathbf{S}_{21}^{geo} = s_3\mathbf{I}_3 \qquad \mathbf{S}_{21}^{mat} = C_{31}\mathbf{f}_1\mathbf{f}_1^T + C_{23}\mathbf{f}_2\mathbf{f}_2^T + C_{33}\mathbf{f}_1\mathbf{f}_2^T + C_{21}\mathbf{f}_2\mathbf{f}_1^T \tag{A.10}$$

$$\mathbf{S}_{22}^{geo} = s_2\mathbf{I}_3 \qquad \mathbf{S}_{22}^{mat} = C_{33}\mathbf{f}_1\mathbf{f}_1^T + C_{22}\mathbf{f}_2\mathbf{f}_2^T + C_{32}\mathbf{f}_1\mathbf{f}_2^T + C_{23}\mathbf{f}_2\mathbf{f}_1^T \tag{A.11}$$

where s_i is the ith-component of the second Piola-Kirchfoff stress tensor in Voigt notation, $\mathbf{I}_3$ is the identity 3x3 matrix, C_{ij} is a component of the fourth order tensor of elastic moduli in Voigt notation and the vectors $\mathbf{f}_1$ and $\mathbf{f}_2$ constitute the first and second column of the deformation gradient tensor which can be expressed in their transpose forms as:

$$\mathbf{f}_1^T = \begin{pmatrix} 1+g_1 & g_2 & g_3 \end{pmatrix} \qquad \mathbf{f}_2^T = \begin{pmatrix} g_4 & 1+g_5 & g_6 \end{pmatrix} \tag{A.12}$$

References

1. J. Schlaich. On some recent lightweight structures. *Journal of the IASS*, 43(139):69–79, 2002.
2. K. Ishii. *Membrane Structures in Japan*. SPS Publishing Company, Tokio, 1995.
3. H. Berger. Form and function of tensile structures for permanent buildings. *Engineering Structures*, 21:669–679, 1999.
4. H. Berger. *Light Structures. Structures of light*. Birkhuser, 1996.
5. W. J. Lewis. Lightweight tension membranes: an overview. *Civil Engineering*, 126:171–181, 1998.
6. A. E. Green and W. Zerna. *Theoretical Elasticity*. Oxford University Press, 2nd edition, 1968.
7. J. W. Leonard. *Tension structures*. McGraw-Hill, New York, 1988.
8. F. Otto. *Tensile structures*. MIT Press, Cambridge, 1967.
9. S. Timoshenko and S. Woinowsky-Krieger. *Theory of plates and shells*. McGraw-Hill, New York, 1959.
10. M. A. Crisfield. *Non-linear finite element analysis of solids and structures*, volume 1: Essentials. John Wiley and Sons, 1991.
11. J. T. Oden and T. Sato. Finite strains and displacements of elastic membranes by the finite element method. *International Journal of Solids and Structures*, 3:471–488, 1967.
12. F. Grutmann and R. L. Taylor. Theory and finite element formulation of rubberlike membrane shells using principal stretches. *International Journal for Numerical Methods in Engineering*, 35:1111–1126, 1992.
13. E. A. Souza, D. Peric, and D. R. J. Owen. Finite elasticity in spatial description linearization aspects with 3-d membrane applications. *International Journal for Numerical Methods in Engineering*, 38:3365–3381, 1995.

14. B. Wu, X. Du, and H. Tan. A three-dimensional finite element analysis of membranes. *Computers and Structures*, 59(4):601–605, 1996.
15. R. L. Taylor. Finite element analysis of membrane structures. *Publication CIMNE*, 203:1–34, 2001.
16. J. Bonet, R. D. Wood, J. Mahaney, and P. Heywood. Finite element analysis of air supported membrane structures. *Computer methods in applied mechanics and engineering*, 190:579–595, 2000.
17. T. Belytschko, W. K. Liu, and B. Moran. *Nonlinear finite elements for continua and structures*. John Wiley and Sons, 2000.
18. G. A. Holzapfel. *Nonlinear solid mechanics: a continuum approach for Engineering*. John Wiley and Sons, 2000.
19. J. Bonet and R. D. Wood. *Nonlinear continuum mechanics for finite element analysis*. Cambridge University Press, 1997.
20. R. H. Mallett and P. V. Marcal. Finite element analysis of nonlinear structures. *Journal of the Structural Division*, 94(ST9):2081–2105, 1968.
21. S. Rajasekaran and D. W. Murray. Incremental finite elements matrices. *Journal of the Structural Division*, 99(ST12):2423–2438, 1973.
22. L. A. Crivelli and C. A. Felippa. A three-dimensional non-linear Timoshenko beam based on the core-congruential formulation. *Internationl Journal of Numerical Methods in Engineering*, 36:3647–3673, 1993.
23. P. Broughton and P. Ndumbaro. *The analysis of cable and catenary structures*. Thomas Teldford, London, 1994.
24. R. Levy and W. Spillers. *Analysis of geometrically nonlinear structures*. Chapman and Hall, 1995.